A&A 509, A92 (2010)
DOI: 10.1051/0004-6361/200811111


Astronomy & Astrophysics

# Faculae at the poles of the Sun revisited: infrared observations

J. Blanco Rodríguez[1,2] and F. Kneer[2]

[1] CICGE, Observatório Astronómico Prof. Manuel de Barros, Fac. Ciências da Universidade do Porto, Alameda Monte da Virgem, 4430-146 Vila Nova de Gaia, Portugal
e-mail: jblanco@fc.up.pt
[2] Institut für Astrophysik, Friedrich-Hund-Platz 1, 37077 Göttingen, Germany
e-mail: kneer@astro.physik.uni-goettingen.de

Received 8 October 2008 / Accepted 17 September 2009

**ABSTRACT**

*Aims.* This study extends earlier investigations on faculae and their small-scale magnetic fields near the solar poles (polar faculae – PFe) to measurements of the magnetically sensitive infrared (IR) Fe I lines at 1.5 $\mu$m, which provide more accurate information about the magnetic field than lines in the visible spectral range.
*Methods.* PFe were observed with the Tenerife Infrared Polarimeter (TIP II) mounted at the Vacuum Tower Telescope/Observatorio del Teide/Tenerife. Several areas at various heliocentric angles were scanned. Faculae near the solar equator (equatorial faculae – EFe) were also observed for comparison with PFe. The full Stokes vector of the Fe I line pair at 1.5 $\mu$m was measured. The magnetic field properties were determined (1) from the centre of gravity (COG); (2) with the weak field approximation (WFA); (3) assuming the strong field regime (SFR); and (4) with inversions under the hypothesis of Milne-Eddington (ME) atmospheres. Line-of-sight (LOS) velocities were determined from the COG of $I$ profiles and from the zero-crossing of the $V$ profiles.
*Results.* The main findings of this work can be divided in five parts: (1) the detected PFe do not harbour sufficient magnetic flux to account for the global flux observed with other methods. (2) Near the solar limb, the apparent, measured transversal field components are most times stronger than the longitudinal components by factors of up to 10 for both PFe and EFe, as found from observations with *HINODE SOT*. (3) Many PFe indeed harbour kilo-G magnetic fields. Of those, more than 85% possess the same magnetic polarity as the global field. The inclinations $\gamma$ of the strong fields, $|B| \geq 900$ G in the SFR, are compatible with their vertical emergence from the solar surface. (4) The results for weaker fields, $|B| \leq 600$ G from ME inversions, indicate a random magnetic field orientation. (5) The velocities from $I$ profiles and $V$ zero-crossings are in average $\sim$0.3 km s$^{-1}$ towards observer, for both PFe and EFe. The zero-crossings of $V$ exhibit a large velocity dispersion, of up to 3 km s$^{-1}$.

**Key words.** Sun: faculae, plages – magnetic fields – Sun: infrared – techniques: polarimetric

## 1. Introduction

The role of faclulae at the poles of the Sun, i.e. polar faculae (PFe), in the solar magnetic cycle has been evident since the early work of Waldmeier (1955, 1962), Sheeley (1964, 1966), and Makarov & Sivaraman (1989). The maximum occurrence of PFe, down to heliographic latitudes of $|\psi| = 60°$, is offset in time by 5−6 years with respect to the sunspot cycle. As shown by Homann et al. (1997), Okunev (2004), and Okunev & Kneer (2004), PFe harbour kilo-Gauss magnetic fields. The cycle variation in the magnetic flux at the solar poles was modelled by, e.g. Wang et al. (2002), Wang & Sheeley (2003), and Baumann et al. (2004). The models were extended to star spots by Işık et al. (2007).

The relevance of PFe to the total magnetic flux from the polar areas and to the fast wind from the polar coronal holes is unclear. Blanco Rodríguez et al. (2007, henceforth Paper I) found from high-spatial resolution measurements that the small-scale PFe contain too little magnetic flux to account for the global flux measured by low-resolution magnetography (Svalgaard et al. 1978; Benevolenskaya 2004) or in the solar wind from the solar poles (Smith & Balogh 1995). We refer to this earlier study (Paper I) for a more detailed discussion of the properties of PFe and more references. Recently, Tsuneta et al. (2008) have analysed *HINODE SOT* data from the south polar cap of the Sun and estimated magnetic fluxes to be consistent with those from the solar wind data.

Our previous investigation was based on observations of the photospheric, visible Fe I 6173 Å line using the "Göttingen" Fabry-Perot spectropolarimeter (FPI, Paper I). The two-dimensional (2D) polarimetric (Stokes $I$ and $V$) data were analysed with speckle methods yielding high spatial resolution better than 0.″5. Yet the polarimetric sensitivity of these earlier observations, from August 2005, allowed us to detect magnetic field strengths down to just $|B_{\rm LOS}| \geq 60$ G ($3\sigma_B$), because of the measurement of $V$ on two different parts of the detector, without beam exchange (but see the improvement from the FPI upgrade described in Bello González & Kneer 2008).

In the present study, we extend the investigation of PFe with observations in the infrared wavelength range at 1.56 $\mu$ with the Tenerife Infrared Polarimeter (TIP II, Collados et al. 2007) attached to the Vacuum Tower Telescope (VTT) at the Observatorio del Teide/Tenerife. Image reconstruction is not a viable technique for these data, since TIP II makes use of the slit spectrograph at the VTT, and the spatial resolution is consequently limited to approximately 1″. However, the Zeeman splitting, and therefore the magnetic sensitivity, of the Fe I line pair at 1.56 $\mu$m is large. A further advantage of using TIP II is that it measures the full Stokes vector with high polarimetric

sensitivity, by means of a modulation scheme with ferroelectric liquid crystals.

In addition to studying PFe, we compare below their properties with those of equatorial faculae (EFe) observed close to the west limb.

The set of observations and their parameters are described in Sect. 2. Section 3 deals with the data reduction and the methods used to obtain the facular properties, i.e. magnetic fields and velocities. The results are discussed in Sect. 4. Statistical analyses of PFe and EFe, their areas, magnetic field strengths, and polarities, as well as the velocities in faculae are performed. As in Paper I, the numbers of PFe are also counted to extrapolate from the observed fields of view (FOVs) to the polar cap surfaces and thus to extrapolate to the total magnetic flux in the polar areas of the Sun. The conclusions from this study are presented in Sect. 5.

## 2. Observations

The present work is based on observations from May 15, 2007. They were obtained with TIP II mounted on the VTT at the Observatorio del Teide/Tenerife. The observations were supported by the Kiepenheuer Adaptive Optics System (KAOS, von der Lühe et al. 2003). The seeing was quite stable and good during the whole day, with values of the Fried parameter $r_0 \approx 10$ cm in the visible. The two photospheric Fe I lines in the 1.56 $\mu$m wavelength range (1.5648 $\mu$m, Landé factor $g = 3$, and 1.5652 $\mu$m, $g_{\rm eff} = 1.53$) were recorded. A spectrograph slit of 60 $\mu$m width was chosen. The exposure time was 250 ms and 5 accumulations, i.e. 5 complete cycles of the four polarimeter states of TIP, were taken to increase the signal-to-noise ratio.

Twenty-eight areas with faculae were scanned, 11 close to each of the solar poles and 6 close to the west limb at equatorial latitudes, at different heliocentric angles $\vartheta$. Around the poles, $\mu = \cos\vartheta$ varied between $\mu = 0.53$ and $\mu = 0.30$. Near the equatorial limb, faculae were observed between $\mu = 0.56$ and $\mu = 0.39$. The step size for the spatial scanning perpendicularly to the slit was kept fixed at 0.35″, approximately two times the pixel size along the slit. The size of the fields of view (FOVs) depended on the number of spatial positions observed, which varied between 15 and 40, and included from one to several faculae. The total scanned area near the west limb was approximately 1/3 of those at each pole. Scans of darks, flat fields, and polarimetric calibration frames for correcting instrumental polarisation crosstalks were also taken.

## 3. Data analysis

The usual data reduction, i.e. dark and flat fielding correction, was applied to the data. A continuum correction was performed to take into account the transmission curve of the prefilter. Several continuum positions along the spectral range were selected and the transmission curve was inferred from them with a spline interpolation. Signatures of bad pixels were removed by interpolating from intensities of adjacent pixels and applying a low-pass filter. The four polarimetric states recorded by the TIP modulation were demodulated and the two beams of the polarimeter were combined. The crosstalks were corrected for with the polarimetric calibration data. Most of these corrections were performed with the routines implemented into the TIP software by M. Collados (Instituto de Astrofísica de Canarias).

An example of spectrograms derived from an area containing PFe is presented in Fig. 1. One can clearly see the large separation between the $V$ extrema in one PF resulting from a strong magnetic field. At the same position, the $Q$ profile exhibits large separations between its three lobes. Other $V$ profiles have very strong asymmetries, and one of the $V$ signatures does not possess a noticeable counterpart in $Q$. We note that at this position the magnetic field is weaker than where one sees strong separations of the $V$ lobes and that the field has opposite polarity to the global magnetic field at the (north) pole from where the spectrograms were taken. Also note, in the left panel of Fig. 1 the reversed sign of the $Q$ profile at a short distance (<1″) below the strong $Q$ profile. An example of the four reduced 1.5648 $\mu$m Stokes profiles from a PF at a heliocentric angle $\vartheta = 69°$ ($\mu = 0.36$) is shown in Fig. 2. The profiles are low-pass filtered. The noise in $(Q, U, V)$, determined at continuum wavelengths, is $\sigma \approx 0.001 I_{\rm c}$, where $I_{\rm c}$ is the continuum intensity of Stokes $I$.

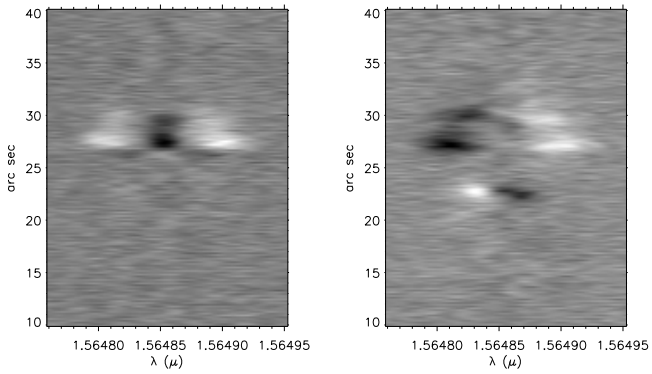


**Fig. 1.** Examples of $Q$ (*left*) and $V$ (*right*) spectrograms around the Fe I 1.5648 $\mu$m line from a scanned area with PFe at $\mu = 0.53$.

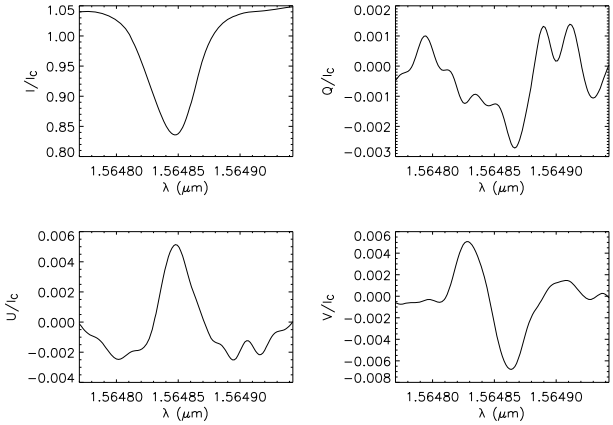


**Fig. 2.** Examples of the Stokes profiles $I$, $Q$, $U$, and $V$, after reduction, around the Fe I 1.5648 $\mu$m line from a PF at $\mu = 0.36$.

The wavelength dispersion of the spectrograms was measured from the comparison between the tabulated wavelength positions of the Fe I line pair and the observed positions. The result was 14.4 mÅ/pixel.

### 3.1. Measurement methods

Velocities are determined in two ways. In the first, parabolae were fitted to the intensities around the minima of the observed $I$ profiles. Their minimum positions gave velocities averaged over the resolution element, including magnetic and non-magnetic structures. The second method uses the zero-crossing of the $V$ profiles. Whenever the Gaussian fits to the $V$ profiles were possible (see Sect. 3.1.1 below), the resulting fit profile

allowed us to determine its zero crossing. As the reference zero of the wavelength displacement, the average position of the line minima for all points in the specific FOV being studied was used.

Four different methods were used to measure magnetic fields, i.e. their strength and polarity: the centre of gravity (COG) method, the weak field approximation (WFA), the strong field regime (SFR), and inversions based on the hypothesis that the Milne-Eddington (ME) approximation describes the facular and surrounding atmospheres and the line formation.

The COG method uses the separation of the centres of gravity of the $\frac{1}{2}(I_\lambda + V_\lambda)$ and $\frac{1}{2}(I_\lambda - V_\lambda)$ profiles and provides a good approximation of the line-of-sight (LOS), or longitudinal, component $\overline{B}_\mathrm{L}$ of the magnetic field averaged over the spatial resolution element and the formation height of the magnetic signal (Semel 1967; Rees & Semel 1979). WFA and SFR are mutually exclusive. For the observed width of the the 1.5648 $\mu$m line, $v_B = \Delta\lambda_\mathrm{D}/\Delta\lambda_B = 1.0$ at ~350 G, where $\Delta\lambda_B$ and $\Delta\lambda_\mathrm{D}$ are the magnetic splitting and the Doppler width, respectively. COG, WFA, and SFR were applied only to the data of the 1.5648 $\mu$m line with Landé factor $g = 3$. However, both IR lines were used in the ME inversions. For more detailed descriptions of these methods, we refer to, e.g. Paper I, Bello González et al. (2005), Lagg et al. (2004), and references therein.

#### 3.1.1. Weak field approximation – WFA

We define the constant $C = -4.67 \times 10^{-13} g_\mathrm{eff} \lambda_0^2$ in units Å G$^{-1}$. In the WFA, the LOS component of the magnetic field can then be inferred from the Stokes $V$ profiles by the expression

$$V(\lambda) = C\,\overline{B}_\mathrm{L} \frac{\mathrm{d}I_0(\lambda)}{\mathrm{d}\lambda}, \tag{1}$$

where $I_0$ is the intensity profile of the $I$ profile without magnetic field. The amplitudes of the $V$ lobes are measured from least square fits of two Gaussians to the $V$ profiles (see, e.g. Okunev 2004; Blanco Rodríguez 2008). The fit allows us to distinguish magnetic signatures from background noise. However, the fitting procedure was successful for only 10% of the pixels in the FOVs. Thus, another least squares calculation, derived from Eq. (1), was also performed giving

$$\overline{B}_\mathrm{L} = \frac{\sum_i V(\lambda_i)\, C'(\lambda_i)}{\sum_i \left(C'(\lambda_i)\right)^2}, \tag{2}$$

where $C'(\lambda_i) = C\,\mathrm{d}I_0(\lambda_i)/\mathrm{d}\lambda$.

Since we measured the full Stokes vector, the transversal component of the magnetic field $B_\mathrm{T}$ can be obtained from the Stokes parameters for linear polarisation, $Q$ and $U$. Again in the WFA, these parameters are related to the second derivative of the intensity in the form

$$Q(\lambda) = -\frac{1}{4}\left(g_\mathrm{eff}\, C\, \lambda_0^2\, B \sin\gamma\right)^2 \cos 2\chi \frac{\mathrm{d}^2 I_0(\lambda)}{\mathrm{d}\lambda^2} \tag{3}$$

$$U(\lambda) = -\frac{1}{4}\left(g_\mathrm{eff}\, C\, \lambda_0^2\, B \sin\gamma\right)^2 \sin 2\chi \frac{\mathrm{d}^2 I_0(\lambda)}{\mathrm{d}\lambda^2}, \tag{4}$$

where $\gamma$ and $\chi$ denote, respectively, the inclination of the magnetic field with respect to the LOS and the azimuth of the projection of the magnetic field onto a plane perpendicular to the LOS. Combining these two expressions for $Q$ and $U$ in Eqs. (3) and (4), the transversal component of the magnetic fields are calculated from

$$B_\mathrm{T} = B \sin\gamma = \frac{1}{D}\left(Q^2 + U^2\right)^{\frac{1}{4}}, \tag{5}$$

where

$$D = \left[\frac{1}{16} C^4 \left(\frac{\mathrm{d}^2 I_0}{\mathrm{d}\lambda^2}\right)^2\right]^{1/4}. \tag{6}$$

Equations (3) and (4) can also be used for least square fits. One can eliminate the azimuth $\chi$ and after some algebra obtains the expression for the transversal magnetic field component

$$\overline{B}_\mathrm{T}^4 = \left(\frac{1}{\frac{1}{4}C^2}\right)^2 \times \frac{\left(\sum_i Q(\lambda_i) I_i''\right)^2 + \left(\sum_i U(\lambda_i) I_i''\right)^2}{\left(\sum_i (I_i'')^2\right)^2}, \tag{7}$$

where $I_i'' = \mathrm{d}^2 I_0(\lambda)/\mathrm{d}\lambda^2$ at wavelength position $\lambda_i$. In the above equation, an averaging over the resolution element is included. In contrast to $\overline{B}_\mathrm{L}$, the averaging in Eq. (7) occurs on the $Q$, $U$ signals, which are proportional to $B_\mathrm{T}^2$ in the WFA. Thus, different from $\overline{B}_\mathrm{L}$, the measured transversal magnetic field is proportional to $\sqrt{f}$, where $f$ is a filling factor of the magnetic field in the resolution element. These dependences on $f$ were pointed out by Lites et al. (2008). In this investigation, we consider, as traditionally assumed, that the filling factors in the spatial resolution element are identical for all four Stokes components ($I$, $Q$, $U$, $V$), although there is no definite reason why.

We note, as emphasised by Landi Degl'Innocenti (1992), that Eqs. (3) and (4) are approximately correct at the line centre wavelength, but that their extension to the full $Q$ and $U$ profiles and the subsequent Eqs. (5)–(7) have no physical justification. However, test calculations for Milne-Eddington cases with analytic solutions have shown that least square fits with Eq. (7) can retrieve the transversal field component to an accuracy superior to 20% even for magnetic splitting two times larger than the Doppler width. The accuracy is higher for lower field strengths. The application of Eq. (7) for the transversal field component is more reliable for these strong fields than the WFA for the longitudinal component $B_\mathrm{L}$ by applying Eq. (2). For weak fields, the longitudinal and transversal components are indeed found to be proportional to $f$ and $\sqrt{f}$, respectively.

The least squares determinations of $B_\mathrm{L}$ and $B_\mathrm{T}$ yielded values at all pixels in the FOVs. We also note that, according to Eq. (7), noise does not enter the determination of $\overline{B}_\mathrm{T}$ quadratically before summation, as it would when averaging in Eq. (5).

#### 3.1.2. Strong field regime – SFR

In SFR, the separation of the Stokes $V$ extrema is proportional to the magnetic field strength.

From the PFe with strong fields, one can also measure the field inclinations and the filling factors. It was noted by Khomenko et al. (2003) that for weak lines and strong fields, i.e. in the Sears limit (Sears 1913), the inclination $\gamma$ of the field versus the LOS can be derived from

$$\frac{A_\mathrm{V}}{\sqrt{A_\mathrm{Q}^2 + A_\mathrm{U}^2}} = \frac{\cos\gamma}{\sin^2\gamma}, \tag{8}$$

where $A_\mathrm{V}$, $A_\mathrm{Q}$, and $A_\mathrm{U}$ are the amplitudes of the Gaussians obtained from the fits to the profiles, $A_\mathrm{V}$ corresponds to the $\sigma$ components, and $A_\mathrm{Q}$ and $A_\mathrm{U}$ correspond to the central $\pi$ component. Khomenko et al. (2003) show that for fields below 600 G, the inclinations are measured to be too low, for the 1.5648 $\mu$m line.

Furthermore, Khomenko et al. (2003) estimate the filling factor $f$ to be

$$f = \frac{2A_\mathrm{V}/I_\mathrm{c}}{(1 - I_0/I_\mathrm{c})\cos\gamma}, \tag{9}$$

where $A_V$ is again the amplitude of the $\sigma$ component from the Gaussian fit, $I_c$ is the continuum intensity, and $I_0$ is the observed residual intensity at line minimum.

#### 3.1.3. Milne-Eddington (ME) inversion

We performed ME inversions with the full Stokes profiles from PFe. The *HELIX* code provided by Lagg et al. (2004) was used. We assumed a two-component atmospheric model for the PFe observations, a magnetic atmosphere with motions, and a surrounding atmosphere that is static. The following parameters were fitted:

- source functions possessing a linear dependence on optical continuum depth $S = S_0 + S_1 \tau$, and assumed to be identical inside and outside the magnetic structure;
- Doppler width $\Delta\lambda_D$, damping constant $\Gamma$, and ratio $\eta$ of line to continuum opacity, which were all different inside from outside the magnetic structure, but identical for the two lines; a further parameter $W$, proportional to the equivalent width, is needed to fit the strength of the 1.5652 $\mu$m line;
- magnetic field parameters, i.e. strength $|B|$, azimuth $\chi$ about the LOS, and inclination $\gamma$ versus LOS in the magnetic structure;
- filling fraction $f$ of magnetic structure in the spatial resolution element;
- macroscopic velocity $v$ inside the magnetic structure;
- additional unpolarised stray light from outside entering the resolution element.

The parameters $\Delta\lambda_D$, $\Gamma$, $\eta$, $W$, $|B|$, $\chi$, $\gamma$, $f$, and $v$ are assumed to be independent of depth. The weights of the Stokes ($I$, $Q$, $U$, $V$) profiles for the inversion were taken to be unity (see Eq. (25) in Lagg et al. 2004). The stray light is an additional intensity added to the Stokes $I$ profile. It is independent of wavelength, e.g. from scattering in the spectrograph. We note that the filling of the spatial resolution element is assumed to be identical for the longitudinal and the transversal field component.

## 4. Results

To identify the faculae present in each FOV in a semi-automatic manner, three thresholds were applied. For a structure to qualify as either a PF or EF, it must possess a LOS magnetic field strength, measured with the COG method, higher than 18 G ($\approx 3\sigma_B$, $\sigma_B$ = standard deviation of noise in LOS magnetic field measurement). Its continuum intensity has also to be $I_{PF,c} \geq 1.02 \times \overline{I_c}$, where $\overline{I_c}$ is the continuum intensity averaged over the scanned area. Finally, to avoid spurious signals, a PF (or EF) needs to have a minimum size of three contiguous pixels, which corresponds to $4.5 \times 10^4$ km$^2$. Here, only structures fulfilling all three of these threshold conditions are considered to be faculae, despite magnetic structures with no associated brightness being found, as well as brightenings harbouring no detectable magnetic field.

### 4.1. Number of PFe, magnetic polarity, and area distributions

Because of the limited area coverage from the observations with the scanning of the FOVs, the number counts and total areas of faculae must be extrapolated to the total area of the polar caps, in order to obtain information about the influence of the PFe on the global field characteristics. We considered as the total area for extrapolation a spherical cap comprising the latitudes $\psi$ of facular occurrence, i.e. from 60° latitude to the pole,

$$F_{PC} = \int_{60°}^{90°} 2\pi R_\odot^2 \cos\psi \mathrm{d}\psi \approx 4.1 \times 10^{11}\ \mathrm{km}^2, \quad (10)$$

the extrapolated numbers of faculae and their total extrapolated areas are presented in Table 1 for north and south poles.

**Table 1.** Extrapolated facular counts and areas.

| | Counts | Areas [$10^8$ km$^2$] |
|---|---|---|
| North pole, total | 4365 | 24.7 |
| magn. positive | 1440 | 4.5 |
| magn. negative | 2925 | 20.2 |
| South pole, total | 2720 | 18.8 |
| magn. positive | 1630 | 13.9 |
| magn. negative | 1090 | 4.9 |

PFe of both magnetic polarities are clearly present at both poles. However, there is a preponderance of one polarity over the other depending on the region of occurrence of the faculae. The polarity with the larger total facular area is the same as the polarity of the global magnetic field at the corresponding pole.

At the date of the observations for this study, active regions were present not far from both west and east limbs at near-equatorial latitudes, although apart from the scanned equatorial areas. We note without showing that in EFe approximately equal numbers and areas are found for both magnetic polarities, as expected. EFe exhibit $V$ profiles with a strong separation between their extrema, an indication of kilo-G fields, while $V$ profiles from their surroundings have smaller lobe separations.

An asymmetry between the two poles can be clearly seen in the facular counts and total areas of Table 1. This indicates a difference between the magnetic flux from the two poles emerging from PFe. An asymmetry in magnetic fluxes from north and south poles was already observed by Benevolenskaya (2004) with data from SoHO MDI. The ratios of the number of faculae with one polarity over those with opposite polarity are very similar for both regions, that is 1.5−2. We also note the high number counts of faculae, which are much higher than observed in early studies by, e.g. Sheeley (1964, 1966).

The same characteristics, numbers and areas were measured in a previous study using the Fe I 6173 Å line in the visible spectral range (Paper I). The number counts of PFe and the ratios of their polarities are very similar for the north pole in both this previous and the present work (the south pole measurements were affected by an observational bias in that study since it dealt with only very few observations from the south pole). Also the PFe areas with the polarity of higher counts are larger than those of opposite polarity. Yet the total areas are much larger by factors 3−6 in the present work. This is due to the lower spatial resolution of the TIP II data than those from the FPI observations in Fe I 6 173 with subsequent image reconstruction. Apparently, the lower spatial resolution of the TIP II observations, of ∼1″, compared with the FPI data in Paper I (∼0.″5) is compensated by the higher polarimetric sensitivity of TIP II. Thus, the apparent area of a PF becomes larger with decreasing spatial resolution, but the polarimetric signal from the magnetic structure remains detectable. A similar behaviour of no dependence of magnetic flux detection on spatial resolution is seen in quiet Sun data, as shown in a comparison between TIP II and high spatial resolution observations by Bello González et al. (2009, their Table 3).

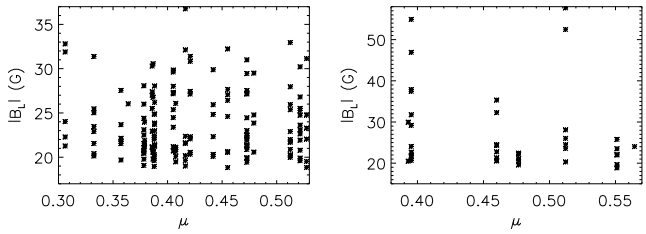


**Fig. 3.** Variation in the longitudinal component of the magnetic field towards the limb for PFe (*left*) and EFe (*right*). Averages of the magnetic field over each facula are represented.

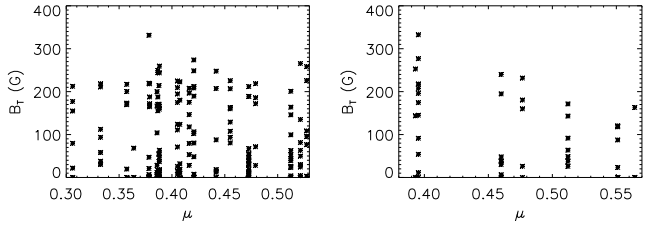


**Fig. 4.** Variation in the transversal component of the magnetic field towards the limb for PFe (*left*) and EFe (*right*). Asterisks represent the average of the magnetic field over each facula.

### *4.2. Magnetic field strengths and field inclinations*

#### 4.2.1. Apparent line-of-sight and transversal components

We now consider all facular fields, irrespective of their actual strengths, while, in Sects. 4.2.3 and 4.2.4, we discriminate between strong and weak fields. Thus, for the moment, the apparent transversal field components $B_{\mathrm{T,meas}}$ were determined in the framework of the WFA by applying Eq. (7). This provides us with first insights into the properties of the transversal field components relative to the longitudinal components.

For the longitudinal, LOS component $B_{\mathrm{L,meas}}$, the amplitude determination of the $V$ profiles by means of fitting Gaussians and then the application of the WFA Eq. (1), failed at 90% of the pixels in the FOVs because of too low signals. Similarly, the application of Eq. (2) to noisy, low-amplitude $V$ profiles produced noisy magnetograms of the LOS field. We therefore present LOS components from our COG determination, which worked everywhere in the FOVs and closely agreed with results from WFA fits when the latter were successful.

Figures 3 and 4 then show the apparent longitudinal and transversal field components, measured at various $\mu = \cos\vartheta$, for both PFe and EFe. A variation in $B_{\mathrm{L,meas}}$ and $B_{\mathrm{T,meas}}$ towards the limb (centre-to-limb variation – CLV) is not seen in the PFe data. The number of observed EFe is low, especially for $\mu \geq 0.45$, and no observations at $\mu < 0.39$ were obtained. Thus, we refrain from commenting on the CLV of the magnetic field components of EFe.

In Fig. 5 of Paper I, we presented the CLV of LOS field components of PFe, measured with an FPI-based spectropolarimeter in Fe I 6173 Å, and found no variation with $\mu$. The LOS field components in that work were a factor of approximately four larger than in the present study of TIP II observations. The reason is that the FPI data are of higher spatial resolution because of image reconstruction, and $B_{\mathrm{L,meas}}$ was thus determined with higher filling factors.

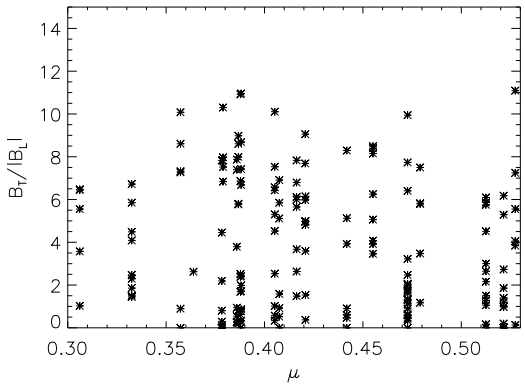


**Fig. 5.** Centre-to-limb variation in the ratio of the transversal to the longitudinal component of the magnetic field. Averages over each PF are presented.

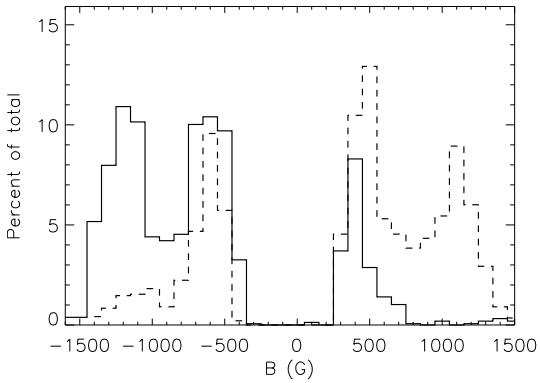


**Fig. 6.** Histograms of magnetic field strengths from the separation of Stokes $V$ extrema of the 1.5648 $\mu$m line. Solid lines correspond to northern PFe, while dashed lines represent southern PFe.

#### 4.2.2. Ratio of horizontal to vertical field strengths

Figure 5 depicts the ratio $B_{\mathrm{T,meas}}/B_{\mathrm{L,meas}}$ of the measured transversal to longitudinal field components from PFe. This ratio varies from close to zero to ∼10. The average ratio is ∼4. Apparently, as for the components themselves, there is no CLV of this ratio. A similar behaviour, a factor of five stronger transversal than longitudinal (apparent) field components, and no CLV was found by Lites et al. (2008) from *HINODE SOT* data for the quiet Sun. The absence of a CLV, as well as the strong variation in the ratio of the transversal to longitudinal field component within one observed FOV, i.e. for a fixed $\mu$, are indications of the strong variation in the field inclination with respect to both the LOS and the vertical direction in the solar atmosphere. We return to this point in Sect. 4.2.4.

#### 4.2.3. Strong field regime – SFR

The total field strength in PFe is also measured in this work by considering the SFR, i.e. by means of the separation of the extrema of the Stokes $V$ profiles. The result of this measurement is presented in Fig. 6 as histograms for both the northern PFe (solid histogram) and the southern PFe (dashed histogram). The ordinate of the histograms corresponds to the percentage of the total number of facular counts separately for north and south pole.

In contrast to the results of a similar analysis for the visible Fe I 6173 Å line with the FPI instrument (cf. Fig. 6 in Paper I), the histograms in Fig. 6 are bimodal in $|B_{\mathrm{SFR}}|$. They exhibit distinct peaks at 400–600 G and at approximately 1 200 G. No

(apparent) field strengths below approximately 250 G are expected since the separation of the $V$ extrema has a lower limit, given by the inflexion points of the Stokes $I_0$ profiles in the WFA.

The histograms in Fig. 6 are remarkable for several reasons:

1. it has been possible to demonstrate directly with the strongly Zeeman-sensitive infrared line at 1.5648 $\mu$m that PFe *may* harbour kilo-G magnetic fields. This was earlier inferred indirectly from lines in the visible spectral range (Homann et al. 1997; Okunev & Kneer 2004) and confirmed by Tsuneta et al. (2008) from Milne-Eddington inversions of *HINODE SOT* measurements in the Fe I 6302 Å line pair;
2. the magnetic polarity in the overwhelming part, >85%, of PFe with strong fields is of the same sign as that of the global magnetic field around the solar poles;
3. not all bright structures at the poles with magnetic fields identified as PFe exhibit strong fields, above one kilo-G. Many have lower field strengths in the 500 G range or lower;
4. the bimodality indicates the existence of two populations of PFe, one with field strengths ≥1000 G and one with a distribution around 500 G with fields also in the range of 250 G and with a possible extension into the kG range;
5. the fields of lower strength are more balanced in polarity than those with strong fields, although not completely.

In the case of the 6173 Å line analysed in Paper I, the SFR method always measured fields above 1000 G. This is an intrinsic limitation of the SFR method when applied to the 6173 Å line. For weak fields (~500 G for this line), the SFR method measures the separation of the inflection points in the intensity profile $I_0(\lambda)$, yielding kG field strengths. Thus, the lower peak of magnetic field strength obtained in the present study was hidden. Figure 6 of Paper I shows peaks of $|B_{\rm SFR}|$ at 1500−1600 G. There, PFe of magnetic polarity opposite to that of the global field were also seen, with more opposite polarity PFe occurring in the southern polar cap than in the northern cap. A similar behaviour is also gathered from the infrared lines in the present study.

The finding in Fig. 6 has consequences for the estimate of the total magnetic flux from the polar caps. In Paper I, we adopted magnetic field strengths of 1500 G for all PFe. Yet here, we find that approximately 50% of the PFe have fields of 500 G and lower. This aggravates the problem of the missing flux in PFe compared to the total flux from the poles of the Sun.

From the bimodality of the histograms in Fig. 6, we infer the existence of two types of PFe, one with weak fields (≤900 G) and another with strong fields (>900 G). Thus, we restrict the remainder of the discussion of the SFR results to field strengths $|B| \geq 900$ G. The two formulae given in Eqs. (8) and (9) in Sect. 3.1.2 were used to find the CLV of both the inclination of the magnetic field with the LOS and the filling factor $f$ in Fig. 7.

The inclinations of strong fields increase with decreasing $\mu$, as $\vartheta$ increases. The dash-dotted line in the left-hand panel of Fig. 7 gives the naive expectation of the linear increase $\gamma = \vartheta$ for fields emerging vertically from the solar surface. Most of the measured $\gamma$ values are located below this line. The average trend of $\gamma$ with $\vartheta$ is depicted by the regression line in the same figure. The right-hand panel in Fig. 7 shows the variation in the filling factors with $\vartheta$ measured by means of Eq. (9). They attain values of ~0.05−0.38. No trend with $\vartheta$ is observed.

The behaviour of too low inclinations $\gamma$ compared with the heliocentric angle $\vartheta$ may occur for two reasons: 1) a LOS effect in diverging magnetic fields, emerging vertically from the solar surface, may give more weight to $V$ signals from the disc centre

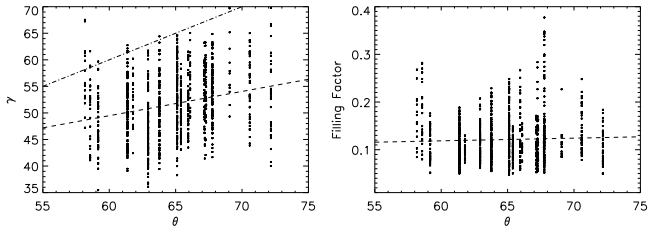


**Fig. 7.** Measurements of PFe with strong fields. Left: variation in inclination $\gamma$ of magnetic field, irrespective of the magnetic polarity, versus LOS with heliocentric angle $\vartheta$. The dashed line is a linear fit to the measurements, and the dash-dotted line represents the expected angle for purely vertical fields. Right: filling factors vs. $\vartheta$, where the dashed line is a linear fit.

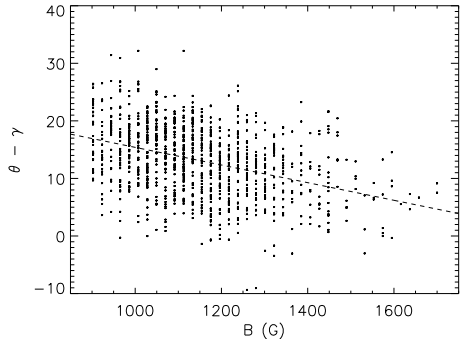


**Fig. 8.** Difference between heliocentric angle $\vartheta$ and inclination angle $\gamma$ versus magnetic field strength measured based on the assumption of SFR, where dashed line is a linear fit.

side of small-scale faculae than from the "axis" of the magnetic structure. This is also reflected by magnetograms from both observation and modelling, where the Stokes $V$ signal is shifted towards disc centre side with respect to the broadband facular brightening (Okunev & Kneer 2004, 2005; Steiner 2005). This shift increases towards the limb, i.e. with increasing $\vartheta$. Further modelling of radiative transfer in magnetic flux tubes should be performed to test this explanation; 2) the determination of $\gamma$ from Eq. (8) becomes increasingly inaccurate with decreasing field strength, in the sense, that fields below the Sears limit yield too small inclinations $\gamma$. This is demonstrated in Fig. 8 where the measured difference $\vartheta - \gamma$ as function of $|B|$, measured based on the assumption of SFR, is depicted (see also Khomenko et al. 2003). The dashed regression line in Fig. 8 shows this dependence. Note that underestimated values of $\gamma$ yield too low filling factors according to Eq. (9). For example, if $\gamma$ is estimated to be 50° instead of 65°, the filling factor is too low by 35%.

In conclusion, for strong fields we find that the measured field inclinations $\gamma$ versus LOS are compatible with *strong* fields emerging vertically from the solar surface.

#### 4.2.4. Estimates from Milne-Eddington (ME) inversion

The magnetic field structure in PFe of strength $|B| < 900$ G *from the SFR determinations*, Fig. 6, was estimated with ME inversions as outlined in Sect. 3.1.3. Figure 9 depicts the inclination $\gamma$ between LOS and magnetic field versus $|B|$. Only results with $|B| > 150$ G are shown. Because of noise, the errors in the determined field strengths for weak fields were too large to provide reliable information. We note that the ME inversions from some Stokes profiles, which give $|B| \leq 900$ G *from the SFR determinations*, result in field strengths also as high as 1200 G.

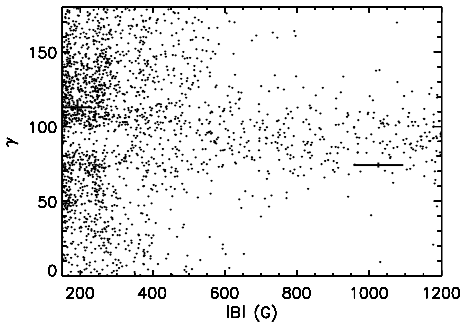


**Fig. 9.** Inclination $\gamma$ between LOS and magnetic field versus $|B|$ from ME inversions. Only results with $|B| < 900$ G from the SFR determinations, Fig. 6, are shown. Error bars indicate the range of variation in the determined quantities from the noise in the data (see text for details).

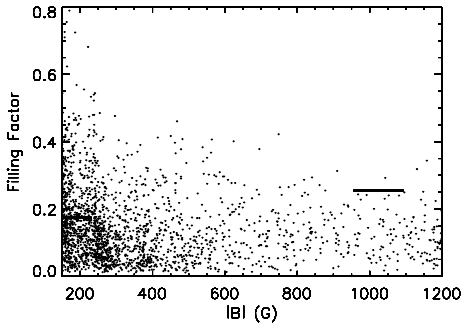


**Fig. 10.** Filling factor versus $|B|$ from ME inversions. Only results with $|B| < 900$ G from the SFR determinations, Fig. 6, are shown. Error bars give the range of variation of the determined quantities from the noise in the data (see text for details).

To estimate the errors in the inversions from noisy data, apart from the uncertainties inherent in the ME approximation, we applied the inversion code by Socas-Navarro (2009, private comm.) to the 1.5468 $\mu$m line (with $g = 3$). Following Socas-Navarro's suggestion, we repeated for a few previously measured Stokes profiles the inversions some 25 times with different initial guesses for the ME parameters. These guesses were taken from normal distributions about the retrieved parameters with rms values of reasonable amplitude. For example, if an inclination of $\gamma = 120°$ was retrieved, i.e. $\gamma > 90°$, a value of 80° was unlikely. The standard deviations of the 25 sets of field strength $|B|$, inclination $\gamma$, and filling factor $f$ found in this way are given as error bars in Fig. 9 as well as in Fig. 10. According to these estimates, $|B|$ is accurate to 70 G for fields in the 1 000 G range and to 40 G for $|B| \approx 200$ G. For strong fields, $\gamma$ and $f$ are well determined, within ±2° and ±0.004, respectively, while for fields of 200 G, they are less accurately known, ±5° and ±0.02, respectively.

For (retrieved) field strengths in the range of 600−1200 G, the inclinations $\gamma$ are distributed between 40° and 140°. The observations were obtained at heliocentric angles of 58°−72°. Purely vertical fields would thus correspond to inclinations of 58°−72° and 108°−122°. In this range of field strengths, we conclude that the magnetic fields tend to be oriented vertically with respect to the solar surface, as already suggested above for strong fields with $|B| \geq 900$ G.

The field inclination (vs. LOS) appears to be increasingly distributed at random with decreasing field strength. Since most of the PF fields are in the range $|B| < 600$ G, this random orientation explains the lack of variation towards the limb of the (apparent) longitudinal and transversal components, $|B_L|$ and $B_T$ in Figs. 3 and 4, respectively. The absence of a centre-to-limb variation in $|B_L|$ was discussed in Paper I, the tentative interpretation being that it was caused by random field orientation.

Figure 10 depicts the filling factors $f$ versus $|B|$ from ME inversions, again with error bars determined as described above. For fields with strengths in the range 600−1200 G, the filling factors were found approximately to be between 0.05 and 0.3, as similarly determined by applying the SFR (cf. right-hand panel in Fig. 7). There is a trend for weaker fields to have larger filling factors, i.e. to be more diffuse than strong fields.

### 4.3. Total magnetic flux

We estimate the total magnetic flux $\Phi_{PFe}$ from PFe at the north pole as follows. From Fig. 6 we adopt for PFe with strong fields an average field strength of $\overline{B} = 1200$ G and from Fig. 7, right panel, an average filling factor of $\overline{f} = 0.15$. We assume that the strong fields are vertically oriented in the solar atmosphere. Based on this assumption, the magnetic field determination in the framework of the SFR and the determination of the filling factor in the Sears limit from the weak 1.56 $\mu$m line are independent of the atmospheric structure of the PFe. We certainly miss strong fields with signals below the detection limit because they are of very small scale, as well as strong-field, mixed polarity structures with cancelling flux that do not contribute to the total flux anyway. Table 1 provides an *upper* limit of the total (extrapolated) area of PFe $A_{PFe} \approx 2 \times 10^{19}$ cm$^2$ with the same polarity as the global magnetic field at the north pole. We neglect that part of the flux is cancelled by opposite polarity fields. We then arrive at a flux estimate of

$$\Phi_{PFe} = F_{PFe} \cdot \overline{f} \cdot \overline{B} \approx 3.6 \times 10^{21}\,\mathrm{Mx}. \quad (11)$$

This value is close to the estimate of total flux, $3.9 \times 10^{21}$ Mx, from the solar north pole, obtained in Paper I from measurements of the Fe I 6173 Å line with a filling factor of $f = 0.3$. Again as in Paper I, the flux from PFe falls short by a factor of approximately 10 from that obtained with measurements at low spatial resolution by Svalgaard et al. (1978) and with field measurements in the solar wind by the *Ulysses* spacecraft (Smith & Balogh 1995). Similar values to that in Eq. (11) were derived from *HINODE SOT* measurements at the south polar cap by Tsuneta et al. (2008). These authors obtained a total magnetic flux that agrees with the flux in the solar wind if they adopt a filling factor $f \equiv 1$ instead of those determined from their Milne-Eddington inversions.

### 4.4. Velocities

Velocities in faculae were obtained from the COG method applied to the Stokes $I$ profiles and from the zero-crossings of the $V$ profiles.

Figure 11 shows the behaviour of velocities towards the limb inferred from the $I$ profiles for PFe (left panel) and EFe (right panel). The regression lines point to some variation that differs for PFe and EFe. However, the intrinsic variations within each FOV prevent us from being able to draw this conclusion.

Figure 12 depicts the histograms for the PFe velocities irrespective of their heliographic position. We show the velocities from both COG $I$ and $V$ zero-crossings separately for the northern and the southern PFe. The mean velocity is in all cases 0.3−0.4 km s$^{-1}$ towards observer, with respect to the average position of the line minima in the FOVs, similar as the result obtained from the Fe I 6173 Å measurements in Paper I. Whether

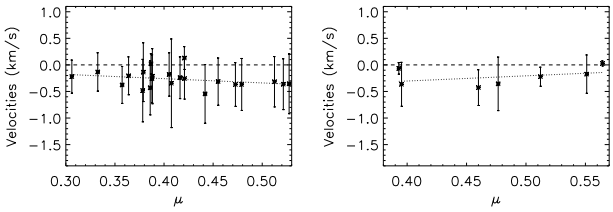


**Fig. 11.** Variation towards the limb of velocities (from COG) of $I$ profiles in polar faculae (*left*) and equatorial faculae (*right*). Asterisks represent the mean velocities of faculae in each FOV. The error bars correspond to the standard deviation of the velocities in the same FOV. The dotted lines are linear fits. The reference zero velocity is the average of all line positions (from COG) in the corresponding FOVs.

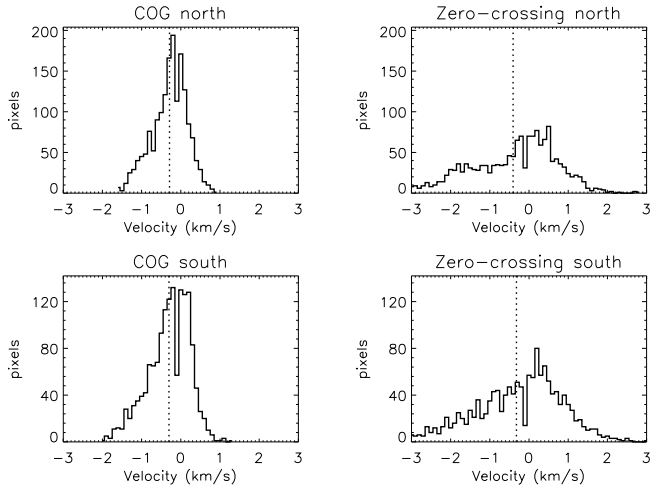


**Fig. 12.** Histograms of velocities in PFe obtained with the COG method for north and south PFe (*top left* and *bottom left*, respectively) and from the zero-crossings of the $V$ profiles (*top right* and *bottom right*, respectively). The vertical dashed lines denote average velocities relative to the average of the line minimum positions in the FOV. Negative velocities correspond to motions *towards* observer.

these average line shifts are indicative of a true, net outflow from PFe remains to be tested by numerical simulations of facular dynamics and of their ambient convection flows. It is unclear how the convective gas flows close to faculae influence the shifts of $I$ and $V$. We note without showing that EFe exhibit very similar velocity distributions. This comparison of velocities from PFe with those from EFe casts doubt on the earlier suggestion that the fast solar wind from the polar coronal holes may be rooted in PFe (Okunev & Kneer 2005, Paper I).

On the one hand, the distributions of the COG shifts from the infrared lines appear narrower, without reaching high velocities, than those measured for the 6173 Å line (see Fig. 8 in Paper I). This is possibly due to the lower spatial resolution of the data in the present analysis than of those in Paper I, thus to a greater spatial averaging. On the other hand, the velocities from the zero-crossings exhibit a broad distribution, with excursions of up to 3 km s$^{-1}$. Figure 13 gives examples with large shifts of the $V$ profiles, demonstrating the high dynamical behaviour of faculae, of the gas contained in them, and of their ambient areas.

## 5. Conclusions

The aim of this work was to widen the knowledge about polar faculae (PFe), to compare them with equatorial faculae (EFe), and to study their magnetic topology. To this end,

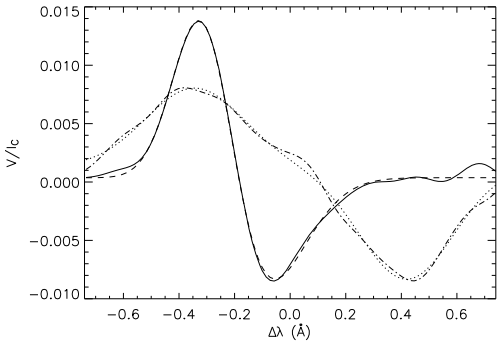


**Fig. 13.** Examples of Stokes $V$ profiles from PFe with strong shifts of their zero-crossings. Solid and dashed profiles correspond to the original data and the fit to two Gaussians, respectively, with strong blue shift; dash-dotted and dotted lines represent the original data and fit, respectively, with strong redshift.

spectropolarimetric observations of the full Stokes vector were taken from PFe, EFe, and the neighbouring photosphere in the magnetically sensitive IR Fe I line pair at 1.5 $\mu$m.

An analysis in which the magnetic features were treated irrespective of their intrinsic field strength found no dependence of the apparent line-of-sight (LOS) and transversal field components on the heliocentric angle. This is an indication that the magnetic fields are more randomly oriented than vertically, i.e. perpendicular to the solar surface.

The strong Zeeman sensitivity allowed us to measure the field strengths in some PFe directly from the separation of the Stokes $V$ lobes with the following results:

1. We were able to prove directly that many PFe harbour magnetic fields in the range of 900−1500 G.
2. A large fraction (>85%) of PFe with these strong fields have the same polarity as the global magnetic field at the poles.
3. Following the work of Khomenko et al. (2003), field inclinations with respect to the LOS and filling factors in the strong field structures could be determined. The result is compatible with the picture of strong fields emerging vertically from the solar surface, which differs from the results for the analysis that does not take into account the intrinsic field strength. The filling factors were found to be in the range 0.05−0.35.
4. The histograms of field strengths from PFe are bimodal. We speculate that there are two types of faculae, those with strong fields in the range of 900−1500 G and those with weaker fields, <900 G.

For faculae with weaker fields, the ones with $|B| < 900$ G from the determination in the SFR, inversions based on Milne-Eddington (ME) atmospheres were applied using the *HELIX* code provided by Lagg et al. (2004). This allowed the determination of the "true" magnetic field strengths $|B|$, inclination angles $\gamma$ versus LOS, and filling factors $f$. One must keep in mind that in this inversion method, the filling of the spatial resolution element is assumed to be identical for both the longitudinal and the transversal field components. To our knowledge, all presently available ME inversion methods applied to the full Stokes profiles implicitly make this assumption, although this situation is realised in only very special magnetic field configurations.

The results from the inversions can be summarised as follows:

1. PF magnetic fields with strengths in the range of 600−1200 G tend to be oriented vertically with respect to the solar surface.

2. The inclinations with respect to the LOS of weaker fields are found to be spread over all angles, compatible with a random orientation. Since most of the PF fields possess strengths of few hundred G, this explains the absence of a variation towards the limb in both the longitudinal and transversal field components in PFe as found in Figs. 3 and 4, and as already discussed in Paper I (Blanco Rodríguez et al. 2007).
3. The filling factors for fields with 600−1200 G are in the range of 0.05−0.3. They tend to increase with decreasing field strength. Thus, weak fields in PFe appear to be diffuse, while strong fields are concentrated.

As in our earlier investigation (Paper I) with high spatial resolution observations in the Fe I 6173 Å line, we extrapolated the magnetic flux in PFe measured from the IR data, to the polar magnetic caps. Again, the total flux in PFe is too small by a factor of 10 to account for the polar magnetic flux measured in magnetograms with low spatial resolution (Svalgaard et al. 1978) or from magnetic field measurements by the *ULYSSES* spacecraft in the solar wind above the poles (Smith & Balogh 1995). Tsuneta et al. (2008) used *HINODE SOT* measurements in visible spectral lines for Milne-Eddington inversions and, only by adopting a large filling factor of $f = 1.0$, obtained total fluxes similar in value to those from the solar wind data. Thus, in our opinion, the magnetism at the poles of the Sun remains enigmatic. It is unclear, whether the flux resides in diffuse magnetic field patches or in strong field concentrations of very small angular scale. Magnetometry in the IR spectral region with much better spatial resolution than presently available is needed to clarify this issue.

*Acknowledgements.* M. Collados and R. Centeno are thanked for their help with TIP II. We thank H. Socas-Navarro for supplying his Milne-Eddington inversion code. J.B.R. acknowledges financial support by Deutsche Forschungsgemeinschaft (DFG) for a PhD grant, 418 SPA-112/15/04, and for a six months postdoc position from grant KN 152/29-3. Also, J.B.R. was partially supported by Fundação para Ciência e Tecnologia through grant PTDCE/CTE-SPA/81678/2003. The Vacuum Tower Telescope is operated by the Kiepenheuer-Institut für Sonnenphysik, Freiburg, at the Spanish Observatorio del Teide of the Instituto de Astrofísica de Canarias.

## References

Baumann, I., Schmitt, D., Schüssler, M., & Solanki, S. K. 2004, A&A, 426, 1075
Bello González, N., & Kneer, F. 2008, A&A, 480, 265
Bello González, N., Okunev, O. V., Domínguez Cerdeña, I., Kneer, F., & Puschmann, K. G. 2005, A&A, 434, 317
Bello González, N., Yelles Chaouche, L., Okunev, O., & Kneer, F. 2009, A&A, 494, 1091
Benevolenskaya, E. E. 2004, A&A, 428, 5
Blanco Rodíguez, J. 2008, Ph.D. Thesis, Göttingen university
Blanco Rodríguez, J., Okunev, O., Puschmann, K. G., Kneer, F., & Sánchez-Andrade Nuño, B. 2007, A&A, 474, 251, Paper I
Collados, M., Lagg, A., Díaz García, J. J., et al. 2007, in The Physics of Chromospheric Plasmas, ed. P. Heinzel, I. Dorotovič, & R. J. Rutten., ASP Conf. Ser., 368, 611
Homann, T., Kneer, F., & Makarov, V. I. 1997, Sol. Phys., 175, 81
Işık, E., Schüssler, M., & Solanki, S. K. 2007, A&A, 464, 1094
Khomenko, E. V., Collados, M., Solanki, S. K., Lagg, A., & Trujillo Bueno, J. 2003, A&A, 408, 1115
Lagg, A., Woch, J., Krupp, N., & Solanki, S. K. 2004, A&A, 414, 1109
Landi Degl'Innocenti, E. 1992, in Solar Observations: Techniques and Interpretation, First Canary Islands Winter School, ed. F. Sánchez, M. Collados, & M. Vázquez (Cambridge, UK: Cambridge Univ. Press), 77
Lites, B. W., Kubo, M., Socas-Navarro, H., et al. 2008, ApJ, 672, 1237
Makarov, V. I., & Sivaraman, K. R. 1989, Sol. Phys., 123, 367
Okunev, O. V. 2004, Ph.D. Thesis, Göttingen university
Okunev, O. V., & Kneer, F. 2004, A&A, 425, 321
Okunev, O. V., & Kneer, F. 2005, A&A, 439, 323
Rees, D. E., & Semel, M. D. 1979, A&A, 74, 1
Sears, F. H. 1913, ApJ, 38, 99
Semel, M. D. 1967, Ann. Astrophys., 30, 513
Sheeley, N. R., Jr. 1964, ApJ, 140, 731
Sheeley, N. R., Jr. 1966, ApJ, 144, 723
Smith, E. J., & Balogh, A. 1995, Geophys. Res. Lett., 22, 3317
Steiner, O. 2005, A&A, 430, 691
Svalgaard, L., Duvall, T. L., Jr., & Scherrer, P. H. 1978, Sol. Phys., 58, 225
Tsuneta, S., Ichimoto, K., Katsukawa, Y., et al. 2008, ApJ, 688, 1374
von der Lühe, O., Soltau, D., Berkefeld, T., & Schelenz, T. 2003, SPIE, 4853, 187
Waldmeier, M. 1955, ZAp, 38, 37
Waldmeier, M. 1962, ZAp, 54, 260
Wang, Y.-M., & Sheeley, N. R., Jr. 2003, ApJ, 599, 1404
Wang, Y.-M., Sheeley, N. R., Jr., & Lean, J. 2002, ApJ, 580, 1188